Nano Energy 82 (2021) 105714

Contents lists available at ScienceDirect

Nano Energy

journal homepage: http://www.elsevier.com/locate/nanoen

Propagating Fe-N_4 active sites with Vitamin C to efficiently drive oxygen electrocatalysis

Chenxi Hu [a,b], Huihui Jin [a,c], Bingshuai Liu [a,b], Lvhan Liang [a,b], Zhe Wang [c], Ding Chen [a,b], Daping He [a,c,*], Shichun Mu [a,b,*]

[a] State Key Laboratory of Advanced Technology for Materials Synthesis and Processing, Wuhan University of Technology, Wuhan 430070, China
[b] Foshan Xianhu Laboratory of the Advanced Energy Science and Technology Guangdong Laboratory, Xianhu hydrogen Valley, Foshan 528200, China
[c] Hubei Engineering Research Center of RF-Microwave Technology and Application, Wuhan University of Technology, Wuhan 430070, China

ARTICLE INFO

Keywords:
Vitamin C
Zeolitic Imidazolate frameworks
Oxygen reduction reaction
Oxygen evolution reaction
Zinc-air batteries

ABSTRACT

Free transition metal ions (such as Fe^{2+}, Co^{2+}) exposed on the surface of metal organic frameworks (MOFs) would be highly aggregated during the carbonization process, which is not conducive to formation of M-N_X active sites, resulting in reduced electrochemically active sites. Accordingly, to effectively suppress the free metal ions on the surface of MOFs and increase Fe-N_4 active sites, Vitamin C (L (+)-ascorbic acid), with an ability to coordinate transition metals, is complexed with ferrous ions. Meanwhile, the acidity of Vitamin C can moderately erode the surface of MOFs materials, further accelerating the generation of holes and defects in the carbonized products. Compared with the control samples without introduction of Vitamin C, the iron-based (VC-MOF-Fe) catalyst, with obviously increased Fe-N_4 active sites, exhibit significantly enhanced oxygen reduction reaction (ORR) and oxygen evolution reaction (OER) performance. When used in rechargeable zinc-air batteries, the peak power density of VC-MOF-Fe (113 mW cm^{-2}) is also better than that of 20% commercial Pt/C + RuO_2. Interestingly, the function of Vitamin C also applies to the cobalt-based catalyst (VC-MOF-Co), evidencing the universality of this strategy.

1. Introduction

Metal-air batteries (such as zinc-air batteries) are regarded as the viable energy in the future due to their high specific energy, easy availability of raw materials and pollution-free [1–4]. However, one of the biggest challenge in practical applications of zinc-air batteries is the slow dynamics of oxygen evolution reaction (OER) and oxygen reduction reaction (ORR) [5–9]. Although Pt/C, IrO_2/RuO_2 and other noble metal cathode catalysts can accelerate the reaction kinetics of ORR and OER, respectively, their high cost, insufficient resources, and poor durability impede the practical application of Zn-air batteries [10–15]. Therefore, exploring efficient and low-cost non-noble catalysts for sustainable and large-scale clean energy equipment is essential.

In recent years, various metal organic frameworks (MOFs) have been developed to prepare metal nanoparticles or metal oxides due to their structural diversity, designability, tailorability and ultra-high specific surface area [16–20]. However, the metal ions exposed on the surface of MOFs incline to condense into larger sizes particles during pyrolysis. The gathering of transition metal ions brings about the reduction in the electrochemically active surface area (ECSA) and interface free energy, which is not conducive to the activity of the catalyst [21,22]. Thus, decreasing the agglomeration of metal particles is indeed important. To avoid this phenomenon, various strategies have been raised, such as lowering the pyrolysis temperature, using oxide coatings, and so on. Meng et al. proposed a method to weaken the agglomeration of metal ions by pyrolyzing ZIF-67 at low temperature with long time processing, but the samples formed had a poor electrocatalytic performance [23]. Lately, our group coated SiO_2 on the surface of ZIF-67 to avoid the rapid agglomeration of Co nanoparticles at high temperatures [24]. However, SiO_2 was difficult to remove completely, and would reduce the electrochemical activity of the final catalysts. Therefore, a facile method needs to be developed to confine the metal ions on the MOF surface, which not only effectively prevents metal ions from aggregation during pyrolysis, but also obtains insufficient degree of graphitization with rich defects and without subsequent purification treatment. In addition, Fe-N_4 is the key active site in the ORR reaction process [25,26], and

* Corresponding authors at: State Key Laboratory of Advanced Technology for Materials Synthesis and Processing, Wuhan University of Technology, Wuhan 430070, China.
E-mail addresses: hedaping@whut.edu.cn (D. He), msc@whut.edu.cn (S. Mu).

https://doi.org/10.1016/j.nanoen.2020.105714
Received 8 November 2020; Received in revised form 16 December 2020; Accepted 17 December 2020

increasing the content of Fe-N_4 active sites is one of the main methods to improve the performance of the catalyst. Undoubtedly, the reduction of ferric (Fe^{3+}) ions in the pyrolysis process promotes the formation of more Fe-N_4 active sites.

Herein, we choose the ZIF series and Vitamin C (L (+)-ascorbic acid) as the carbon source and regulator, respectively. During the preparation of ZIF precursors, when iron salts are added, ferric (Fe^{3+}) ions can be reduced to ferrous (Fe^{2+}) ions by Vitamin C, so as to more easily coordinate with 2-methylimidazole [27]. More importantly, Vitamin C can react with ferrous ions to form a complex ($2C_6H_8O_6 + Fe^{2+} \rightarrow (C_6H_7O_6)_2Fe + 2H^+$), resulting in a decrease in the concentration of exposed free metal ions on the surface of the precursor and the formation of more Fe-N_4 active sites. At the same time, the hydrogen ions generated by the reaction can etch the surface of MOFs, which is beneficial to form holes and defects [28]. As expected, after the introduction of Vitamin C, the as prepared catalyst shows the significantly improved ORR activity under both alkaline and acidic conditions and OER performance in alkaline media. In addition, it can also be applied to long-stable rechargeable zinc-air batteries. The VC-MOF-Co catalyst was also synthesized by the same method, and the ORR and OER performance in alkaline medium were significantly improved, evidencing the universality of this strategy.

2. Experimental section

2.1. Syntheses of VC-Fe/ZIF-8

$Zn(NO_3)_2 \bullet 6H_2O$ (4.0 mmol) was added in 36 mL of methanol

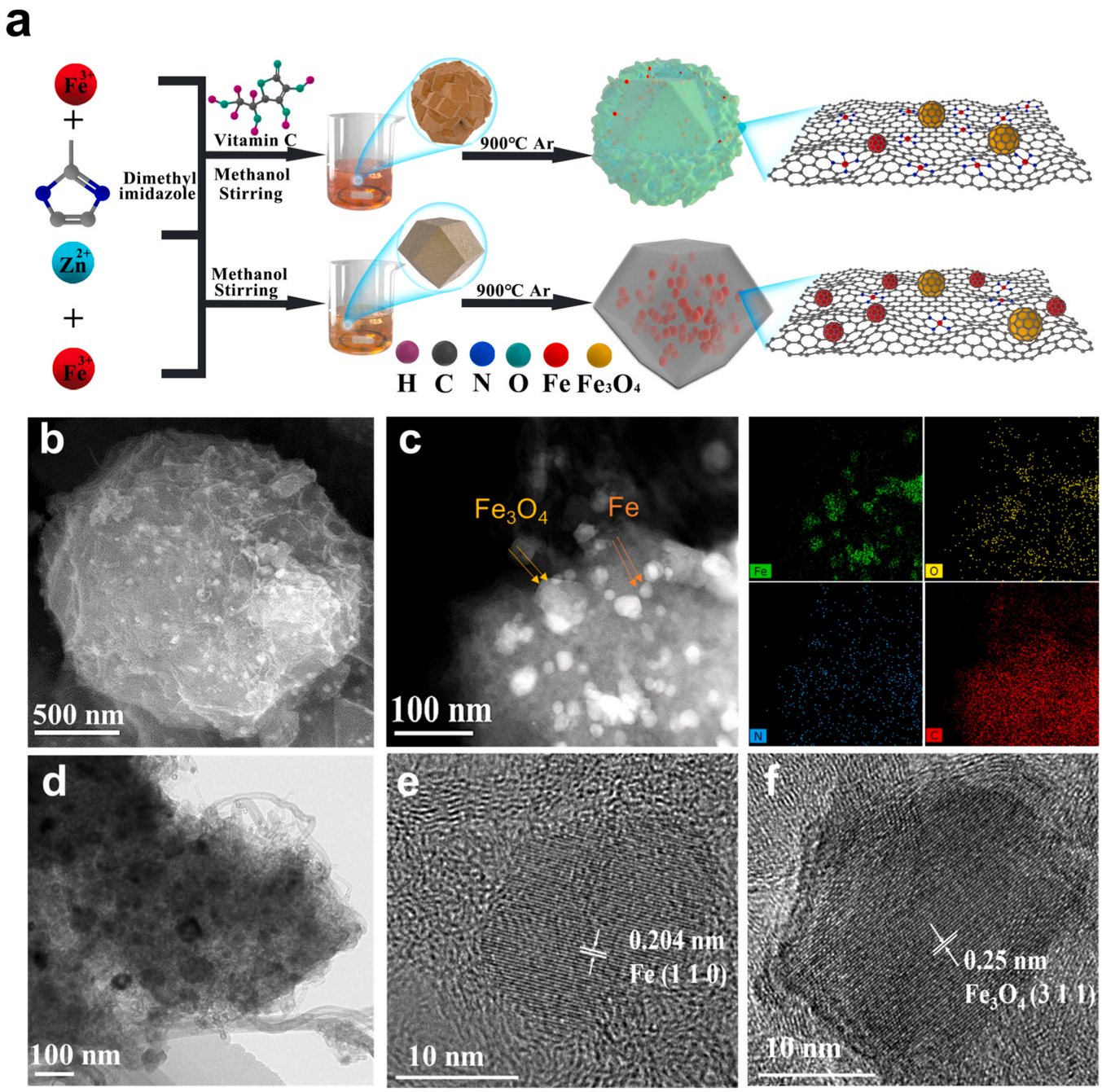

Fig. 1. (a) Schematic synthesis process of VC-MOF-Fe and MOF-Fe; (b) SEM image, (c) STEM image with HAADF-STEM mapping, (d) TEM image, (e, f) HRTEM images of VC-MOF-Fe.

solution, Vitamin C (0.24 mmol) and $Fe(NO_3)_3 \bullet 9H_2O$ (0.25 mmol) were added in 10 mL of deionized water, then mixed the two solutions with 36 mL methanol solution containing 2-methylimidazole (32.0 mmol). After stirring for 24 h, the mixed solution was centrifuged, washed and dried in a vacuum oven to obtain samples.

2.2. Syntheses of VC-MOF-Fe

VC-MOF-Fe was obtained by calcining VC-Fe/ZIF-8 at 900 °C for 3 h in an argon atmosphere. For the synthesis of the remaining samples, please refer to the supporting literature.

3. Results and discussion

3.1. Structural characterization

Before the experiment, the contents of Vitamin C and Fe $(NO_3)_3 \bullet 9H_2O$ were first explored for optimal sample preparation (EIS, Fig. S1a, b). After confirming that the sample (VC-MOF-Fe) prepared with 0.25 mmol of $Fe(NO_3)_3 \bullet 9H_2O$ and 0.24 mmol of Vitamin C had the best ORR activity, the role of Vitamin C in the sample was further probed. The synthesis process of VC-MOF-Fe is represented in Fig. 1**a**. VC-MOF-Fe was obtained by mixing $Fe(NO_3)_3 \bullet 9H_2O$, 2-Methylimidazole, $Zn(NO_3)_2 \bullet 6H_2O$ and Vitamin C in methanol solution, and then calcining at 900 °C under argon atmosphere.

The morphology and structure of all catalysts were investigated with scanning electron microscopy (SEM) and transmission electron microscopy (TEM). Different from Fe/ZIF-8, VC-Fe/ZIF-8 (EIS, Fig. S2a, b) is no longer a regular rhombic dodecahedron. Obviously, the introduction of Vitamin C leads to morphological changes. Then, the XRD patterns of the precursors (EIS, Fig. S3) show that the diffraction peaks of VC-Fe/ZIF-8 and Fe/ZIF-8 are almost the same as those of the original ZIF-8, which indicates that the structure of MOFs has not changed after the introduction of Vitamin C and iron salt. After high temperature pyrolysis, the surface of VC-MOF-Fe forms a depression, with a unique mesoporous structure (Fig. 1**b**), which promotes the reactants to enter the interior of the material and effectively utilize the active sites inside [29], while MOF-Fe maintains the rhombic dodecahedron shape(EIS, Fig. S4). HAADF-STEM mapping images (Fig. 1**c**) further show that N, C and O are highly dispersed, while Fe is mainly distributed as dispersed nanoparticles. As shown in Figs. 1**d,** S5**a**, the nanoparticles are distributed on carbon matrix of VC-MOF-Fe. TEM and HAADF-STEM mapping images of MOF-Fe are displayed in the Supporting Material (EIS, Figs. S5b, S6). In high-resolution TEM (HRTEM) images, the lattice spacings are 0.204 and 0.25 nm, belong to (110) plane of metal Fe particles and (311) plane of Fe_3O_4 particles (Fig. 1**e**, **f**), indicating the presence of Fe and Fe_3O_4 in VC-MOF-Fe.

Fig. 2**a** shows that VC-MOF-Fe and MOF-Fe have three X-ray diffraction (XRD) peaks, which are attributed to C, Fe and Fe_3O_4, respectively, suggesting that iron exists in the form of iron particles and

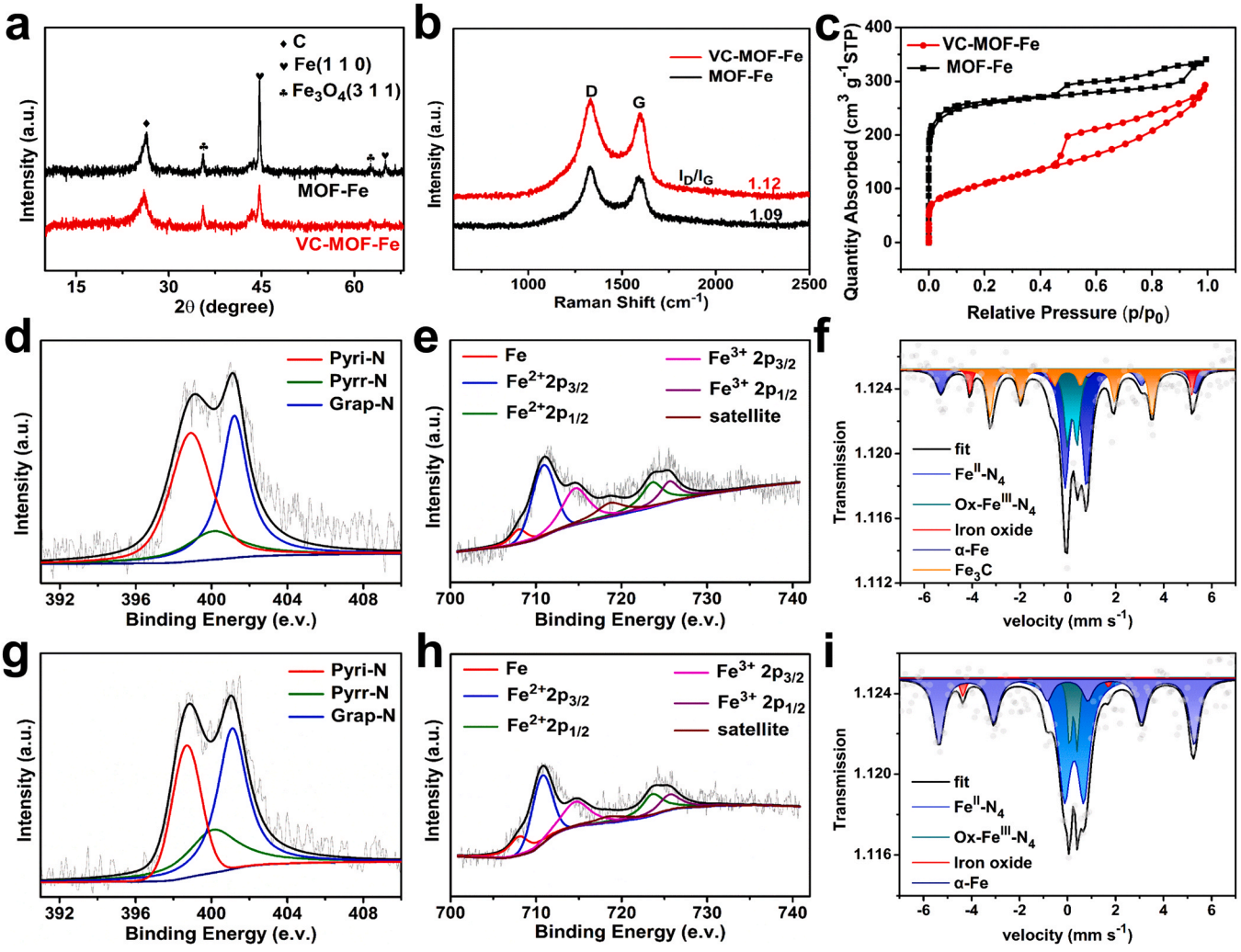

Fig. 2. (a) XRD patterns, (b) Raman spectrum, (c) N_2 sorption isotherms of VC-MOF-Fe and MOF-Fe; (d) N1s, (e) Fe 2p spectra, (f) Fe Mössbauer spectra of VC-MOF-Fe; (g) N1s, (h) Fe 2p spectra, (i) Fe Mössbauer spectra of MOF-Fe.

iron oxides, which is consistent with the results of HRTEM. Compared with MOF-Fe, the diffraction peak intensity of iron element in XRD pattern of VC-MOF-Fe is significantly reduced, implying a decrease in the content of iron particles or particle size. Interestingly, similar rules are also found in VC-MOF-Co and MOF-Co catalysts. After the addition of Vitamin C, the diffraction peak intensity of the cobalt particles decreases significantly (EIS, Fig. S7), indicating that after treatment with Vitamin C, the concentration of exposed free metal ions on the surface of the precursor is obviously reduced.

From Raman spectra (Fig. 2**b**), it shows two distinct peaks, namely D and G band. Notably, the I_D/I_G ratio of VC-MOF-Fe is 1.12, while that of MOF-Fe is 1.09, indicating that abundant defects exist in VC-MOF-Fe [30,31]. Similarly, for N-C-VC, the I_D/I_G ratio is 1.05, greater than that of N-C (1.03) (EIS, Fig. S8), while1.18 for VC-MOF-Co, higher than that of MOF-Co (1.14) (EIS, Fig. S9). The pore structure of samples was studied by N_2 adsorption/desorption test. The adsorption isotherms of VC-MOF-Fe and MOF-Fe (Fig. 2**c**) belong to type IV isotherms, indicating the presence of micropores and mesopores in both samples [32,33]. As analysis from the pore size distribution (EIS, Fig. S10), the number of mesopores increases in VC-MOF-Fe compared with MOF-Fe. The above results manifest that the addition of Vitamin C not only affects the distribution of particles, but also influences the morphology and structure in the catalyst.

The chemical state and basic elements of the sample surface were investigated using XPS. It displays that the catalyst contains N, C, O and Fe elements, which matches the element mapping results. The high-resolution N 1s spectrum of VC-MOF-Fe can be subdivided into three peaks at 401.2, 400.1, 398.9 eV (Fig. 2**d**), which represent pyrrolic N (pyrr-N), pyridinic N (pyri-N) and graphitic N (grap-N), respectively [34,35]. As reported, pyri-N can facilitate the enhancement of the onset potential of the ORR, whereas the grap-N can enhance the diffusion-limited current density [36]. Compared to MOF-Fe (Fig. 2**g**), the amount of pyri-N and grap-N in VC-MOF-Fe is raised, leading to an increase in active sites and limiting current density. The high-resolution Fe 2p spectrum can be deconvoluted into six peaks (Fig. 2**e, h**), namely Fe (708 eV), $Fe2p_{3/2}$ (Fe(II), Fe(III) 710.9–714.6 eV), $Fe2p_{1/2}$ (Fe(II), Fe (III) 723.6–725.6 eV) and satellite peak (718.7 eV), indicating the presence of Fe, Fe(II) and Fe(III) in VC-MOF-Fe and MOF-Fe [37–39]. Especially, compared with MOF-Fe, the content of Fe particles in VC-MOF-Fe is reduced, which is consistent with the XRD result. Meanwhile, the high-resolution C 1s spectrum is divided into five bonding types: carbon hybridized (sp2, 284.5 eV), diamond-like carbon hybridized (sp3, 285 eV), C–N (285.6 eV), C–O (286.6 eV) and C=O (288.3 eV) (EIS, Fig. S11a) [40]. Compared to MOF-Fe (EIS, Fig. S11b), the C–N content of VC-MOF-Fe shows a noticeable increase, indicating that VC-MOF-Fe embraces more active sites. In addition, the high-resolution O 1s spectrum can be subdivided into three peaks at 530.3, 532.3, 533.6 eV (EIS, Fig. S12a, b), which represent Fe–O, OH^- and H–OH, respectively [41,42].

To further determine the chemical state of iron in samples, Mössbauer spectra of Fe were investigated. The fitting parameters are listed in Table S1. The spectrum of VC-MOF-Fe can be divided into five components (Fig. 2**f**): Fe^{II}-N_4, Ox-Fe^{III}-N_4, iron oxides, α-Fe and Fe_3C [43–45]. For MOF-Fe, the spectrum can be divided into four components (Fig. 2**i**): Fe^{II}-N^4, Ox-Fe^{III}-N_4, iron oxide and α-Fe. Compared with MOF-Fe, the content of α-Fe in VC-MOF-Fe significantly decreases, while it slightly increases for the content of iron oxides, which is consistent with the XRD result. Interestingly, the content of Fe-N_4 in VC-MOF-Fe increases, especially the amount of Ox-Fe^{III}-N_4. As reported, Ox-Fe^{III}-N_4 is mainly responsible for ORR activity [46]. Additionally, through both ICP and XPS tests, the Fe content in VC-MOF-Fe and MOF-Fe is consistent (Table S2). Therefore, combined with the Mössbauer spectroscopy result, it further confirms that Vitamin C can react with ferrous ions to form complexes, resulting in a decrease in the concentration of free metal ions exposed on the surface of the precursor and forming more Fe-N_4 active sites.

3.2. Electrocatalytic activity and stability towards ORR

The ORR performance of the as prepared samples was first explored. The cyclic voltammetry (CV) curve (Fig. 3**a**) shows an obvious cathode peak in O_2-saturated electrolyte (0.1 M KOH), implying the high activity of VC-MOF-Fe for reducing oxygen. Linear sweep voltammetry (LSV) curves (Fig. 3**b, c**) indicate that the half-wave potential ($E_{1/2}$) and limiting current density of VC-MOF-Fe are 0.886 V and − 5.80 mA cm^{-2}, respectively, both of which are better than MOF-Fe (0.862 V, − 5.45 mA cm^{-2}) and commercial Pt/C (0.851 V, − 5.62 mA cm^{-2}), demonstrating VC-MOF-Fe has an outstanding ORR performance in alkaline media. Coincidentally, after the addition of Vitamin C to ZIF-8 and ZIF-67, a significant increase in the half-wave potential is also observed (EIS, Fig. S13). Besides, the kinetic current density (J_K) is an important evaluation parameter of ORR activity. When the voltage is 0.9 V and 0.85 V, theJ_K value of VC-MOF-Fe is 3.34 and 17.24 mA cm^{-2}, respectively, which are both greater than MOF-Fe (2.09 and 10.27 mA cm^{-2}). Moreover, VC-MOF-Fe also has a smallest Tafel slope (84 mV dec^{-1}) (the Tafel slopes of MOF-Fe, Pt/C, N-C-VC, N-C are 93, 103, 142, 161 mV dec^{-1}, respectively) (Fig. 3**d**), indicating that its electron transfer rate is much faster [47]. Furthermore, according to K-L equation and LSV curves at different speeds, the electron transfer number of VC-MOF-Fe is 3.97, showing the four-electron oxygen reduction process in VC-MOF-Fe (EIS, Fig. S14a).

Apart from outstanding ORR activity, VC-MOF-Fe also exhibits good stability. After 8 h testing, the normalized current of VC-MOF-Fe only drops by 2.9%, while that of 20% Pt/C decreases 21.6% after 3 h (Fig. 3**e**). Meanwhile, the LSV curves of VC-MOF-Fe were plotted before and after 5000 cycles, the $E_{1/2}$ of VC-MOF-Fe fades by only 4 mV (EIS, Fig. S14b). In methanol-tolerance experiment (Fig. 3f), the current density of VC-MOF-Fe has remained 99.1% after adding 9 mL methanol, while the commercial Pt/C decreases rapidly, suggesting that VC-MOF-Fe has preferable methanol tolerance. Then, SCN^- was further used to poison the metal-centered catalytic sites to detect the Fe-N_4 active site. After adding 0.01 M KSCN, the ORR activity is significantly reduced (EIS, Fig. S15), demonstrating that Fe-N_4 is indeed the active site.

Based on the superb ORR performance of VC-MOF-Fe under alkaline conditions, we further studied its performance in 0.5 M H_2SO_4 solution. The $E_{1/2}$ of VC-MOF-Fe is 0.753 V, slightly lower than 20% Pt/C (0.789 V) but significantly higher than MOF-Fe (0.719 V) (Fig. 3**g**). Electron transfer number of VC-MOF-Fe is 3.96 by using K-L equation (EIS, Fig. S16). In addition, durability and methanol tolerance of catalyst under acidic conditions were also explored by using chronoamperometric curves. After 12 h testing, the normalized current of VC-MOF-Fe only decreases by 12.7%, whereas the commercial Pt/C decreases about 26.2% after only 8 h (Fig. 3**h**), indicating that VC-MOF-Fe has excellent stability. In the methanol-tolerance test (Fig. 3**i**), after adding 9 mL methanol, the current density of Pt/C drops sharply, while VC-MOF-Fe has only 2.1% decaying for the current density, showing its preferable resistance to methanol.

3.3. Electrocatalytic activity and stability towards OER

To assess the OER activity, the LSV curves on VC-MOF-Fe, MOF-Fe and RuO_2 catalysts were recorded in 1 M KOH. Fig. 4**a** shows the IR-compensated LSV curves. The overpotential of VC-MOF-Fe is 339 mV (@10 mA cm^{-2}), which is much better than that of MOF-Fe (432 mV), and comparable to RuO_2 (320 mV) (Fig. 4**b**). Similarly, after the addition of Vitamin C to ZIF-67, the overpotential decreases significantly (EIS, Fig. S17). The OER dynamics of catalysts was further analyzed by Tafel diagrams and presented in Fig. 4**c**. Compared with MOF-Fe (143 mV dec^{-1}), VC-MOF-Fe has a smaller Tafel slope (78 mV dec^{-1}), which is equivalent to RuO_2 (72 mV dec^{-1}), revealing its similar OER kinetic process with RuO_2. The superb OER activity is due to its fast electron transfer, which can be evaluated by electrochemical impedance spectroscopy (EIS) [48]. Compared with MOF-Fe, the electron transfer

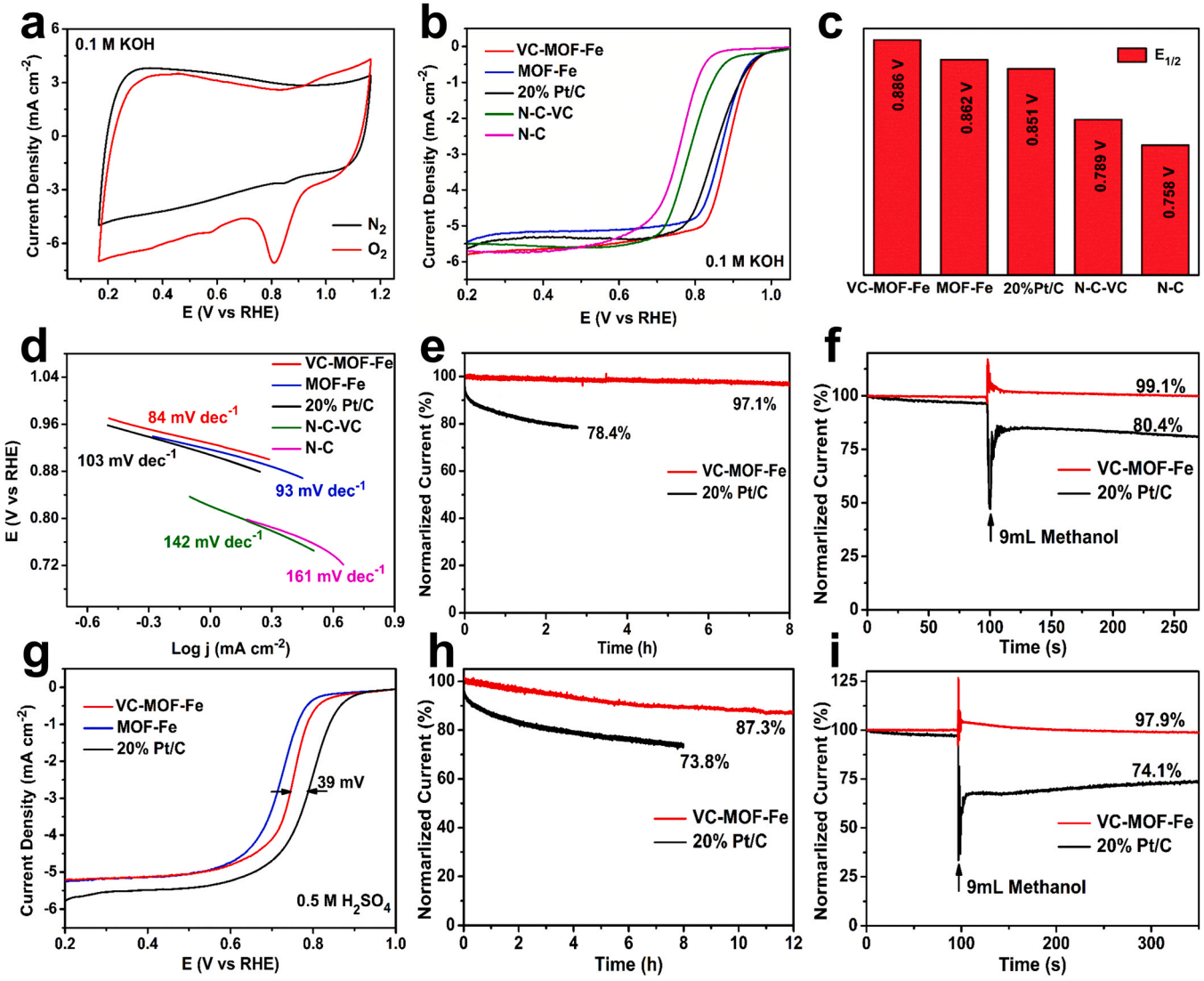

Fig. 3. (a) CV curves in 0.1 M KOH saturated with N_2 and O_2; (b) LSV curves, (c) $E_{1/2}$ comparison, (d) Tafel slopes of VC-MOF-Fe, MOF-Fe, 20% Pt/C, N-C-VC and N-C; (e) Stability test, (f) Methanol resistance test of VC-MOF-Fe and 20% Pt/C in 0.1 M KOH; (g) LSV curves of VC-MOF-Fe, MOF-Fe and 20% Pt/C in 0.5 M H_2SO_4; (h) Stability test, (i) Methanol resistance test of VC-MOF-Fe and 20% Pt/C in 0.5 M H_2SO_4.

resistance of VC-MOF-Fe is significantly low at the open circuit voltage (Fig. 4**d**), showing that the charge transfer of VC-MOF-Fe is faster than other catalysts.

Besides catalytic performance, the stability is also important in practical applications of electrocatalysts. After 2000 CV cycles, the overpotential of VC-MOF-Fe only reduces by 6 mV (Fig. 4**e**), whereas RuO_2 decreases about 15 mV (EIS, Fig. S18). Furthermore, the chronoamperometric response was performed under the overpotential of 350 mV to evaluate the durability of VC-MOF-Fe. Fig. 4**f** displays that the current consumption of VC-MOF-Fe is only 6.9% after 8 h operation, indicating that it has excellent stability. In addition, the phase stability of VC-MOF-Fe shown in Fig. 4**g** after accelerated cycling test further reflects its durability to theOER. XPS analysis (Fig. 4**h**) shows that the peak area of Fe^{3+} increases after CV acceleration, indicating that the continuous OER promotes the gradual oxidation of Fe^{2+} on the electrocatalyst surface [49]. In the same time, a new adsorbed oxygen peak appears in XPS spectrum of O 1s (Fig. 4**i**) at 536 eV [50,51], confirming that the OER would cause oxidation on the catalyst surface.

To further understand the high catalytic performance of VC-MOF-Fe, double layer capacitance (C_{dl}) was measured to represent electrochemically active surface area (ECSA) [52,53]. The fitted C_{dl} of VC-MOF-Fe (33 mF cm^{-2}) is higher than MOF-Fe (31 mF cm^{-2}) (EIS, Fig. S19), indicating that VC-MOF-Fe has a larger electrochemically active surface area.

3.4. Zinc–air battery performance

Based on the excellent bifunctional catalytic performance of the VC-MOF-Fe catalyst (Table S3), and to explore the practical application potential of the catalyst, a rechargeable zinc–air battery was assembled with VC-MOF-Fe as the air cathode and zinc plate as anode, and 20% Pt/C + RuO_2 was fabricated as a comparison (Fig. 5**a**). The zinc-air battery based on VC-MOF-Fe shows the open circuit voltage of 1.49 V, while the 20% Pt/C+RuO_2 is only 1.43 V (Fig. 5**b**). The discharge/charge polarization curves of VC-MOF-Fe is shown in Fig. 5**c**, VC-MOF-Fe exhibits a low potential gap, indicating it has a better recharge ability. The polarization curves (Fig. 5**d**) display that the peak power density of the VC-MOF-Fe-based zinc-air battery is 113 mW cm^{-2}, higher than 20% Pt/C+ RuO_2 (91 mW cm^{-2}). Fig. 5**e** illustrates the galvanostatically discharge curves (@5 mA cm^{-2}), VC-MOF-Fe displays a higher and more stable discharge platform (1.33 V) than 20% Pt/C + RuO_2 (1.28 V). Then, all-solid-state battery was also fabricated, which shows a

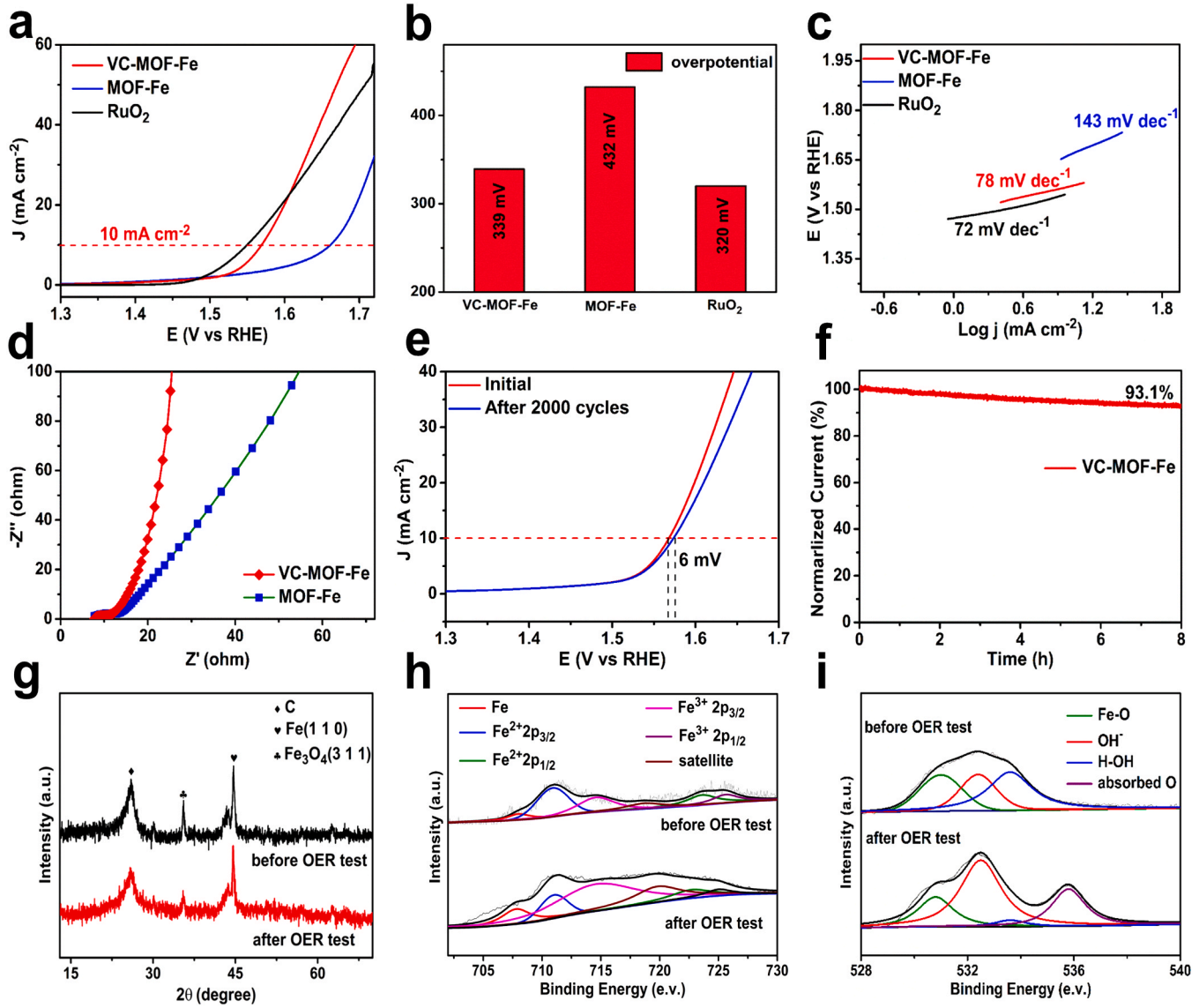

Fig. 4. (a) OER polarization curves, (b) Corresponding overpotentials (j = 10 mA cm^{-2}), (c) Tafel slopes of VC-MOF-Fe, MOF-Fe and RuO_2 in 1 M KOH; (d) Nyquist plots for VC-MOF-Fe and MOF-Fe obtained under the open circuit voltage; (e) Polarization curves of VC-MOF-Fe before and after 2000 CV cycles; (f) Chronoamperometric responses of VC-MOF-Fe; (g) XRD pattern, XPS spectra of (h) Fe 2p and (i) O 1s of VC-MOF-Fe before and after OER test.

high OCV (1.41 V), and three such batteries are able to make a ~3.4 V LED glow (Fig. 5**f**).

Our experimental results demonstrate that VC-MOF-Fe has brilliant electrocatalytic activity with good long-term stability. High activity of VC-MOF-Fe can be attributed to the following points: Firstly, Vitamin C reacts with ferrous ions to form a complex, thereby reducing the concentration of exposed metal ions on the precursor surface, and then increasing Fe-N_4 active sites; Secondly, the surface of VC-MOF-Fe forms a depression and has more mesoporous structure, which increases the contact area and facilitates effective contact between the reactants and active sites of the catalyst; Finally, the presence of rich defects contribute to enhancing conductivity and activity [54,55].

4. Conclusions

In summary, by means of Vitamin C, we successfully designed a facile and novel strategy to reduce the concentration of free metal ions on the surface of MOFs and increase Fe-N_4 active sites by complexing transition metal ions (Fe^{2+}). As expected, for derivatives (VC-MOF-Fe) of MOFs treated with Vitamin C, we can clearly observe a decrease in metal particles content, and an increase of Fe-N_4 active sites, leading to a significant improvement in oxygen electrocatalytic performance. The as prepared VC-MOF-Fe displayed a much enhanced ORR and OER activity and stability. Furthermore, the rechargeable primary zinc-air battery based on VC-MOF-Fe as the air cathode exhibited a higher peak power density, superb durability and a stable discharge platform than 20% Pt/C + RuO_2. In addition, the VC-MOF-Co catalyst was also synthesized with the same method, indicating the generality of this strategy. Therefore, this work opens up new research directions on reducing the agglomeration of surface metal ions, increasing active sites and designing highly efficient electrocatalysts.

CRediT authorship contribution statement

Shichun Mu, Daping He: Conceptualization, Writing - review & editing, Validation. **Chenxi Hu:** Methodology, Writing - original draft preparation. **Huihui Jin**: Software, **Bingshuai Liu, Lvhan Liang**: Data curation. **Zhe Wang**: Visualization. **Ding Chen**: Investigation.

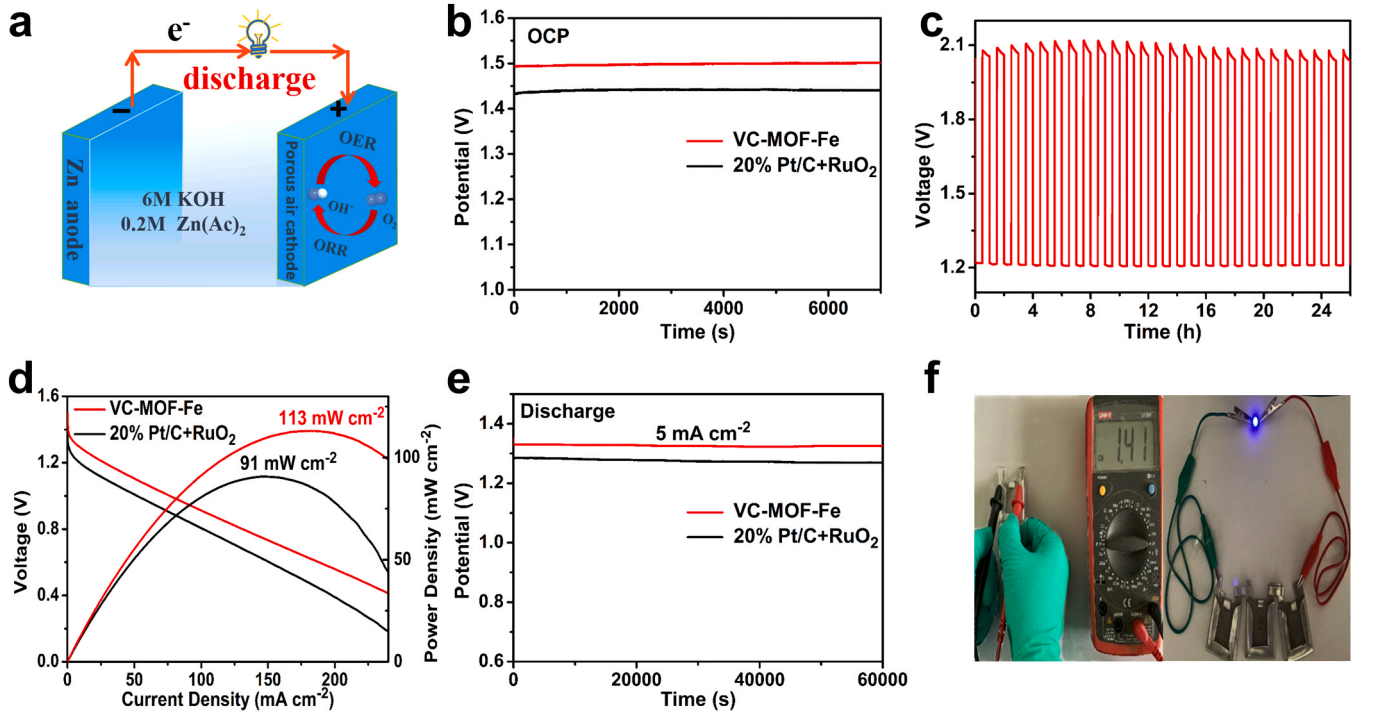

Fig. 5. (a) Schematic diagram of zinc-air battery; (b) Open circuit voltage with VC-MOF-Fe or 20% Pt/C + RuO_2; (c) Galvanostatic discharge and charge cycling performance of VC-MOF-Fe; (d) Polarization curves; (e) Discharge curves at 5 mA cm^{-2}; (f) Photos show an open-circuit voltage of 1.41 V and a lighted LED (~3.4 V) powered by three all solid-state zinc-air batteries inter.

Declaration of Competing Interest

The authors declare that they have no known competing financial interests or personal relationships that could have appeared to influence the work reported in this paper.

Acknowledgments

This work was supported by the National Natural Science Foundation of China (51672204, 51701146, 22075223), and National Key Research and Development Program of China (No. 2016YFA0202603).

Appendix A. Supporting information

Supplementary data associated with this article can be found in the online version at doi:10.1016/j.nanoen.2020.105714.

References

[1] Y. Zang, H. Zhang, X. Zhang, R. Liu, S. Liu, G. Wang, Y. Zhang, H. Zhao, Fe/Fe_2O_3 nanoparticles anchored on Fe-N-doped carbon nanosheets as bifunctional oxygen electrocatalysts for rechargeable zinc-air batteries, Nano Res. 9 (2016) 2123–2137.
[2] G. Fu, X. Yan, Y. Chen, L. Xu, D. Sun, J.-M. Lee, Y. Tang, Boosting bifunctional oxygen electrocatalysis with 3D graphene aerogel-supported Ni/MnO particles, Adv. Mater. 30 (2018), 1704609.
[3] Q. Wang, Y. Lei, Z. Chen, N. Wu, Y. Wang, B. Wang, Y. Wang, Fe/Fe_3C@C nanoparticles encapsulated in N-doped graphene–CNTs framework as an efficient bifunctional oxygen electrocatalyst for robust rechargeable Zn–air batteries, J. Mater. Chem. A 6 (2018) 516–526.
[4] C. Li, M. Wu, R. Liu, High-performance bifunctional oxygen electrocatalysts for zinc-air batteries over mesoporous Fe/Co-N-C nanofibers with embedding FeCo alloy nanoparticles, Appl. Catal. B Environ. 244 (2019) 150–158.
[5] R. Nandan, A. Gautam, S. Tripathi, K.K. Nanda, A comprehensive analysis and rational designing of efficient Fe-based oxygen electrocatalysts for metal–air batteries, J. Mater. Chem. A 6 (2018) 8537–8548.
[6] C.C. Yang, S.F. Zai, Y.T. Zhou, L. Du, Q. Jiang, Fe_3C-Co nanoparticles encapsulated in a hierarchical structure of N-doped carbon as a multifunctional electrocatalyst for ORR, OER, and HER, Adv. Funct. Mater. 29 (2019), 1901949.
[7] P. Prabhu, V. Jose, J.-M. Lee, Design strategies for development of TMD-based heterostructures in electrochemical energy systems, Matter 2 (2020) 526–553.
[8] B. Wang, Y. Ye, L. Xu, Y. Quan, W. Wei, W. Zhu, H. Li, J. Xia, Space-confined yolk-shell construction of Fe_3O_4 nanoparticles inside N-doped hollow mesoporous carbon spheres as bifunctional electrocatalysts for long-term rechargeable zinc–air batteries, Adv. Funct. Mater. 30 (2020), 2005834.
[9] X. Wei, Y. Zhang, B. Zhang, Z. Lin, X. Wang, P. Hu, S. Li, X. Tan, X. Cai, W. Yang, L. Mai, Yolk-shell-structured zinc-cobalt binary metal sulfide@N-doped carbon for enhanced lithium-ion storage, Nano Energy 64 (2019), 103899.
[10] H.B. Yang, J. Miao, S.F. Hung, J. Chen, H.B. Tao, X. Wang, L. Zhang, R. Chen, J. Gao, H.M. Chen, L. Dai, B. Liu, Identification of catalytic sites for oxygen reduction and oxygen evolution in N-doped graphene materials: development of highly efficient metal-free bifunctional electrocatalyst, Sci. Adv. 2 (2016), e1501122.
[11] T. He, B. Lu, Y. Chen, Y. Wang, Y. Zhang, J.L. Davenport, A.P. Chen, C.W. Pao, M. Liu, Z. Sun, A. Stram, A. Mordaunt, J. Velasco, Y. Ping, Y. Zhang, S. Chen, Research (2019), 6813585 (Wash. DC).
[12] H. Jiang, Y. Yao, Y. Zhu, Y. Liu, Y. Su, X. Yang, C. Li, Iron carbide nanoparticles encapsulated in mesoporous Fe–N-doped graphene-like carbon hybrids as efficient bifunctional oxygen electrocatalysts, ACS Appl. Mater. Interfaces 7 (2015) 21511–21520.
[13] X.X. Wang, V. Prabhakaran, Y. He, Y. Shao, G. Wu, Iron-free cathode catalysts for proton-exchange-membrane fuel cells: cobalt catalysts and the peroxide mitigation approach, Adv. Mater. 31 (2019), 1805126.
[14] G. Fu, Y. Wang, Y. Tang, K. Zhou, J.B. Goodenough, J.-M. Lee, Superior oxygen electrocatalysis on nickel indium thiospinels for rechargeable Zn–air batteries, ACS Mater. Lett. 1 (2019) 123–131.
[15] Q. Liang, L. Zhong, C. Du, Y. Luo, Y. Zheng, S. Li, Q. Yan, Achieving highly efficient electrocatalytic oxygen evolution with ultrathin 2D Fe-doped nickel thiophosphate nanosheets, Nano Energy 47 (2018) 257–265.
[16] Y. Feng, H. Wang, S. Zhang, Y. Zhao, J. Gao, Y. Zheng, P. Zhao, Z. Zhang, M. J. Zaworotko, P. Cheng, S. Ma, Y. Chen, Antibodies@MOFs: an in vitro protective coating for preparation and storage of biopharmaceuticals, Adv. Mater. 31 (2019), 1805148.
[17] M.Y. Masoomi, A. Morsali, A. Dhakshinamoorthy, H. Garcia, Mixed-metal MOFs: unique opportunities in metal–organic framework (MOF) functionality and design, Angew. Chem. Int. Ed. 58 (2019) 15188–15205.
[18] Y.P. Wu, W. Zhou, J. Zhao, W.W. Dong, Y.Q. Lan, D.S. Li, C. Sun, X. Bu, Surfactant-assisted phase-selective synthesis of new cobalt MOFs and their efficient electrocatalytic hydrogen evolution reaction, Angew. Chem. Int. Ed. 56 (2017) 13001–13005.
[19] G. Fu, Y. Tang, J.-M. Lee, Recent advances in carbon-based bifunctional oxygen electrocatalysts for Zn–Air batteries, ChemElectroChem 5 (2018) 1424–1434.
[20] B. You, N. Jiang, M. Sheng, S. Gul, J. Yano, Y. Sun, High-performance overall water splitting electrocatalysts derived from cobalt-based metal–organic frameworks, Chem. Mater. 27 (2015) 7636–7642.

[21] D. Mendoza-Cachú, C. Mercado-Zúñiga, G. Rosas, Surfactant assisted stabilization of carbon nanotubes synthesized by a spray pyrolysis method, Adv. Condens. Matter Phys. (2017), 1751768.
[22] F. Lin, Z. Dong, Y. Yao, L. Yang, F. Fang, L. Jiao, Electrocatalytic hydrogen evolution of ultrathin Co-Mo_5N_6 heterojunction with interfacial electron redistribution, Adv. Energy Mater. 10 (2020), 2002176.
[23] J. Meng, C. Niu, L. Xu, J. Li, X. Liu, X. Wang, Y. Wu, X. Xu, W. Chen, Q. Li, Z. Zhu, D. Zhao, L. Mai, General oriented formation of carbon nanotubes from metal–organic frameworks, J. Am. Chem. Soc. 139 (2017) 8212–8221.
[24] H. Zhou, D. He, A.I. Saana, J. Yang, Z. Wang, J. Zhang, Q. Liang, S. Yuan, J. Zhu, S. Mu, Mesoporous-silica induced doped carbon nanotube growth from metal–organic frameworks, Nanoscale 10 (2018) 6147–6154.
[25] R. Ding, Y. Liu, Z. Rui, J. Li, Z. Zou, Facile grafting strategy synthesis of single-atom electrocatalyst with enhanced ORR performance, Nano Res. 13 (2020) 1519–1526.
[26] Y. Wang, L. Wan, P. Cui, L. Tong, Y. Ke, T. Sheng, M. Zhang, S. Sun, H. Liang, Y. Wang, K. Zaghib, H. Wang, Z. Zhou, J. Yuan, Small 16 (2020), 2002203.
[27] X. Wang, H. Zhang, H. Lin, S. Gupta, C. Wang, Z. Tao, H. Fu, T. Wang, J. Zheng, G. Wu, X. Li, Directly converting Fe-doped metal–organic frameworks into highly active and stable Fe-N-C catalysts for oxygen reduction in acid, Nano Energy 25 (2016) 110–119.
[28] X. Wei, X. Luo, H. Wang, W. Gu, W. Cai, Y. Lin, C. Zhu, Highly-defective Fe-N-C catalysts towards pH-universal oxygen reduction reaction, Appl. Catal. B Environ. 263 (2020), 118347.
[29] Z. Wang, H. Jin, T. Meng, K. Liao, W. Meng, J. Yang, D. He, Y. Xiong, S. Mu, Fe, Cu-coordinated ZIF-derived carbon framework for efficient oxygen reduction reaction and zinc-air batteries, Adv. Funct. Mater. 28 (2018), 1802596.
[30] P. Pachfule, D. Shinde, M. Majumder, Q. Xu, Fabrication of carbon nanorods and graphene nanoribbons from a metal–organic framework, Nat. Chem. 8 (2016) 718–724.
[31] D. Geng, Y. Chen, Y. Li, R. Li, X. Sun, S. Ye, S. Knights, High oxygen-reduction activity and durability of nitrogen-doped graphene, Energy Environ. Sci. 4 (2011) 760–764.
[32] N. Xu, Y. Zhang, T. Zhang, Y. Liu, J. Qiao, Efficient quantum dots anchored nanocomposite for highly active ORR/OER electrocatalyst of advanced metal-air batteries, Nano Energy 57 (2019) 176–185.
[33] K. Waki, R.A. Wong, H.S. Oktaviano, T. Fujio, T. Nagai, K. Kimoto, K. Yamada, Non-nitrogen doped and non-metal oxygen reduction electrocatalysts based on carbon nanotubes: mechanism and origin of ORR activity, Energy Environ. Sci. 7 (2014) 1950–1958.
[34] X.R. Wang, J.Y. Liu, Z.W. Liu, W.C. Wang, J. Luo, X.P. Han, X.W. Du, S.Z. Qiao, J. Yang, Identifying the key role of Pyridinic-N-Co bonding in synergistic electrocatalysis for reversible ORR/OER, Adv. Mater. 30 (2018), 1800005.
[35] X. Hu, Y. Chen, M. Zhang, G. Fu, D. Sun, J.-M. Lee, Y. Tang, Alveolate porous carbon aerogels supported Co_9S_8 derived from a novel hybrid hydrogel for bifunctional oxygen electrocatalysis, Carbon 144 (2019) 557–566.
[36] J. Yang, H. Sun, H. Liang, H. Ji, L. Song, C. Gao, H. Xu, A highly efficient metal-free oxygen reduction electrocatalyst assembled from carbon nanotubes and graphene, Adv. Mater. 28 (2016) 4606–4613.
[37] H. Jin, H. Zhou, W. Li, Z. Wang, J. Yang, Y. Xiong, D. He, L. Chen, S. Mu, In situderived Fe/N/S-codoped carbon nanotubes from ZIF-8 crystals as efficient electrocatalysts for the oxygen reduction reaction and zinc–air batteries, J. Mater. Chem. A 6 (2018) 20093–20099.
[38] Z. Zhang, J. Sun, F. Wang, L. Dai, Efficient oxygen reduction reaction (ORR) catalysts based on single iron atoms dispersed on a hierarchically structured porous carbon framework, Angew. Chem. Int. Ed. 57 (2018) 9038–9043.
[39] W. Jiao, C. Chen, W. You, J. Zhang, J. Liu, R. Che, Yolk-shell Fe/Fe_4N@Pd/C magnetic nanocomposite as an efficient recyclable ORR electrocatalyst and SERS substrate, Small 15 (2019), 1805032.
[40] S. Gao, B. Fan, R. Feng, C. Ye, X. Wei, J. Xu, X. Bu, N-doped-carbon-coated Fe_3O_4 from metal-organic framework as efficient electrocatalyst for ORR, Nano Energy 40 (2017) 462–470.
[41] M. Xiao, Y. Chen, J. Zhu, H. Zhang, X. Zhao, L. Gao, X. Wang, J. Zhao, J. Ge, Z. Jiang, S. Chen, C. Liu, W. Xing, Climbing the Apex of the ORR volcano plot via binuclear site construction: electronic and geometric engineering, J. Am. Chem. Soc. 141 (2019) 17763–17770.
[42] P.F. Liu, X. Li, S. Yang, M.Y. Zu, P. Liu, B. Zhang, L.R. Zheng, H. Zhao, H.G. Yang, $Ni_2P(O)/Fe_2P(O)$ interface can boost oxygen evolution electrocatalysis, ACS Energy Lett. 2 (2017) 2257–2263.
[43] M. Wang, Y. Yang, X. Liu, Z. Pu, Z. Kou, P. Zhu, S. Mu, The role of iron nitrides in the Fe–N–C catalysis system towards the oxygen reduction reaction, Nanoscale 9 (2017) 7641–7649.
[44] J. Li, S. Ghoshal, W. Liang, M.T. Sougrati, F. Jaouen, B. Halevi, S. Mckinney, G. Mccool, C. Ma, X. Yuan, Structural and mechanistic basis for the high activity of Fe–N–C catalysts toward oxygen reduction, Energy Environ. Sci. 9 (2016) 2418–2432.
[45] A.L. Morel, S.I. Nikitenko, K. Gionnet, A. Wattiaux, J. Lai-Kee-Him, C. Labrugere, B. Chevalier, G. Deleris, C. Petibois, A. Brisson, M. Simonoff, Sonochemical approach to the synthesis of Fe_3O_4@SiO_2 core−shell nanoparticles with tunable properties, ACS Nano 2 (2008) 847–856.
[46] M. Xiao, J. Zhu, L. Ma, Z. Jin, J. Ge, X. Deng, Y. Hou, Q. He, J. Li, Q. Jia, S. Mukerjee, R. Yang, Z. Jiang, D. Su, C. Liu, W. Xing, Microporous framework induced synthesis of single-atom dispersed Fe-N-C acidic ORR catalyst and its in situ reduced Fe-N_4 active site identification revealed by X-ray absorption spectroscopy, ACS Catal. 8 (2018) 2824–2832.
[47] G. Fu, X. Jiang, Y. Chen, L. Xu, D. Sun, J.-M. Lee, Y. Tang, Robust bifunctional oxygen electrocatalyst with a "rigid and flexible" structure for air-cathodes, NPG Asia Mater. 10 (2018) 618–629.
[48] H. Yan, Y. Xie, A. Wu, Z. Cai, L. Wang, C. Tian, X. Zhang, H. Fu, Anion-modulated HER and OER activities of 3D Ni–V-based interstitial compound heterojunctions for high-efficiency and stable overall water splitting, Adv. Mater. 31 (2019), 1901174.
[49] B. Song, K. Li, Y. Yin, T. Wu, L. Dang, M. Cabán-Acevedo, J. Han, T. Gao, X. Wang, Z. Zhang, J.R. Schmidt, P. Xu, S. Jin, Tuning mixed nickel iron phosphosulfide nanosheet electrocatalysts for enhanced hydrogen and oxygen evolution, ACS Catal. 7 (2017) 8549–8557.
[50] P. Ji, H. Jin, H. Xia, X. Luo, J. Zhu, Z. Pu, S. Mu, Double metal diphosphide pair nanocages coupled with P-doped carbon for accelerated oxygen and hydrogen evolution kinetics, ACS Appl. Mater. Interfaces 12 (2020) 727–733.
[51] L. Gong, H. Zhang, Y. Wang, E. Luo, K. Li, L. Gao, Y. Wang, Z. Wu, Z. Jin, J. Ge, Z. Jiang, C. Liu, W. Xing, Bridge bonded oxygen ligands between approximated FeN_4 sites confer catalysts with high ORR performance, Angew. Chem. Int. Ed. 59 (2020) 13923–13928.
[52] Z. Feng, E. Wang, S. Huang, J. Liu, A bifunctional nanoporous Ni–Co–Se electrocatalyst with a superaerophobic surface for water and hydrazine oxidation, Nanoscale 12 (2020) 4426–4434.
[53] J. Chen, C. Fan, X. Hu, C. Wang, Z. Huang, G. Fu, J.-M. Lee, Y. Tang, Hierarchically porous Co/CoxMy(M = P, N) as an efficient mott–schottky electrocatalyst for oxygen evolution in rechargeable Zn–Air batteries, Small 15 (2019), 1901518.
[54] Y. Zhao, J. Wan, H. Yao, L. Zhang, K. Lin, Few-layer graphdiyne doped with sp-hybridized nitrogen atoms at acetylenic sites for oxygen reduction electrocatalysis, Nat. Chem. 10 (2018) 924–931.
[55] P. Liu, D. Gao, W. Xiao, L. Ma, K. Sun, P. Xi, D. Xue, J. Wang, Self-powered water-splitting devices by core-shell NiFe@N-graphite-based Zn-Air batteries, Adv. Funct. Mater. 28 (2018), 1706928.

Chenxi Hu received her B.E. degree from Henan University of Science and Technology in 2017. Now she is a master student in fuel cell at Wuhan University of Technology. Her research interests focus on metal-organic frameworks (MOFs) and the development of non-precious metal for electrocatalysis.

Huihui Jin received her B.E., M.Sc and Ph.D. degree in 2013, 2015 and 2020 from Wuhan University of technology. Now she is a postdoctor in Wuhan University of technology. Her current research interests lie in the development of non-precious metal for electrocatalysis and electrochemical sensor.

Bingshuai Liu received respectively his B.E. and B.Ec degree from the School of Materials Science and Engineering and Business School at University of Jinan in 2018. He is currently a research master in school of Material Science and Engineering from Wuhan University of Technology. His research interests focus on metal-organic frameworks (MOFs) and their applications in electrochemical energy storage.

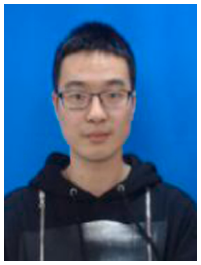

Lvhan Liang received his B.E. degree in 2017 from polymer materials and engineering of Hubei University. Currently he is a research master of State Key Laboratory of Advanced Technology for Materials Synthesis and Processing, Wuhan University of Technology. His current research topic is the construction of heterostructures of supported metal single-atom clusters and the study of electrocatalytic performance.

Zhe Wang is a Ph.D. candidate at School of Science, Wuhan University of Technology (WUT). He received his B.S. and M.S. degree at School of Chemical and Biological Engineering in Changsha University of Science & Technology (2015) and State Key Laboratory of Advanced Technology for Materials Synthesis and Processing in WUT (2018), respectively. His research is mainly focused on graphene-based film materials for electromagnetic interference shielding, strain sensors and mechanics.

Ding Chen received his B.E. degree in 2018 from Huainan Normal University in Material Chemistry. Currently he is a research master of State Key Laboratory of Advanced Technology for Materials Synthesis and Processing, Wuhan University of Technology. Now his research topic is the application of transition metal phosphates in hydrogen production by electrolysis of water.

Daping He is a full professor at Wuhan University of Technology. He obtained his Ph.D. degree in Materials Processing Engineering from Wuhan University of Technology in 2013. He was a Postdoctoral Fellow in the University of Science and Technology of China. Then he joined University of Bath as a Newton International Fellow and University of Cambridge as a Postdoctoral Fellow. His research interest is preparation and application of nano composite materials into new energy devices, sensors and RF microwaves field. He has published over 80 peer-reviewed papers and 20 Chinese patents.

Shichun Mu is Chair Professor at Wuhan University of Technology. He received his Ph.D. degree from Chinese Academy of Sciences, China in 2001. Afterwards, he joined the Wuhan University of Technology as a postdoctoral researcher in 2001–2003. Since 2006, he has been a full professor at Wuhan University of Technology. He was an academic visitor at Inorganic Chemistry Laboratory, University of Oxford in 2007–2008. His research focuses on nanocarbon materials, PEM fuel cell/water splitting electrocatalysts, and metal-air battery, lithium ion battery related materials and devices. He has published over 200 peer reviewed papers.